AD-A123 669 ULF NEAR FIELDS IN LAYERED MEDIA(U) PACIFIC-SIERRA RESEARCH CORP LOS ANGELES CA E C FIELD ET AL. OCT 82 PSR-1225 N00014-82-C-0073 1/1

UNCLASSIFIED F/G 20/14 NL

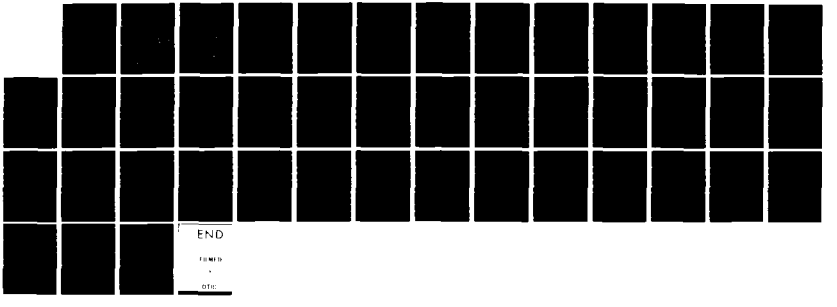

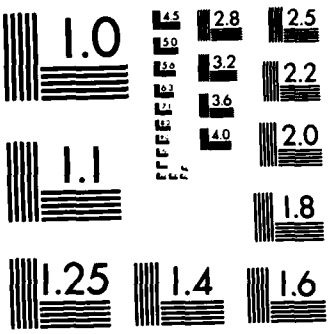

MICROCOPY RESOLUTION TEST CHART
NATIONAL BUREAU OF STANDARDS-1963-A

PSR Report 1225

ULF NEAR FIELDS IN LAYERED MEDIA

E. C. Field, Jr.
C. R. Warber

October 1982

Final Technical Report
Contract N00014-82-C-0073

Sponsored by
Office of Naval Research
800 North Quincy Street
Arlington, Virginia 22217

PACIFIC·SIERRA RESEARCH CORP.
12340 Santa Monica Blvd. • Los Angeles, California 90025

PSR Report 1225

ULF NEAR FIELDS IN LAYERED MEDIA

E. C. Field, Jr.
C. R. Warber

October 1982

Final Technical Report
Contract N00014-82-C-0073

Sponsored by
Office of Naval Research
800 North Quincy Street
Arlington, Virginia 22217

PACIFIC-SIERRA RESEARCH CORP.
12340 Santa Monica Blvd. • Los Angeles, CA 90025 • (213) 820-2200

SECURITY CLASSIFICATION OF THIS PAGE (When Data Entered)

REPORT DOCUMENTATION PAGE

READ INSTRUCTIONS BEFORE COMPLETING FORM

1. REPORT NUMBER: PSR Report 1225	2. GOVT ACCESSION NO.: AD-A123 669
3. RECIPIENT'S CATALOG NUMBER	
4. TITLE (and Subtitle): ULF NEAR FIELDS IN LAYERED MEDIA	5. TYPE OF REPORT & PERIOD COVERED: Final Technical Report November 1981 - November 1982
	6. PERFORMING ORG. REPORT NUMBER: PSR Report 1225
7. AUTHOR(s): E. C. Field, Jr. C. R. Warber	8. CONTRACT OR GRANT NUMBER(s): N00014-82-C-0073
9. PERFORMING ORGANIZATION NAME AND ADDRESS: Pacific-Sierra Research Corporation 12340 Santa Monica Boulevard Los Angeles, California 90025	10. PROGRAM ELEMENT, PROJECT, TASK AREA & WORK UNIT NUMBERS: NR089-164
11. CONTROLLING OFFICE NAME AND ADDRESS: Office of Naval Research 800 N. Quincy Street Arlington, Virginia 22217	12. REPORT DATE: October 1982 13. NUMBER OF PAGES: 35
14. MONITORING AGENCY NAME & ADDRESS(if different from Controlling Office): Leader, Arctic, Atmospheric and Ionospheric Sciences Division Code 420	15. SECURITY CLASS. (of this report): Unclassified 15a. DECLASSIFICATION DOWNGRADING SCHEDULE

16. DISTRIBUTION STATEMENT (of this Report)

Distribution unlimited, cleared for public release

17. DISTRIBUTION STATEMENT (of the abstract entered in Block 20, if different from Report)

18. SUPPLEMENTARY NOTES

19. KEY WORDS (Continue on reverse side if necessary and identify by block number)

ULF propagation
ULF communication
ULF near fields

20. ABSTRACT (Continue on reverse side if necessary and identify by block number)

This report derives formulas for ULF near fields using a five-layer, stratified model of the earth-air-ionosphere system, and gives numerical results for a frequency of 0.1 Hz and ranges between 5 km and 5 Mm. It assumes a semi-infinite, finitely conducting ionosphere 50 km above a three-layer earth, comprising a moderately conductive overburden, a resistive layer, and a highly conductive mantle. It therefore accommodates the two-dimensional confinement of the fields between the earth and the ionosphere as well as possible

DD FORM 1 JAN 73 1473 EDITION OF 1 NOV 65 IS OBSOLETE

SECURITY CLASSIFICATION OF THIS PAGE (When Data Entered)

20. (cont.)

waveguide modes in the resistive layer. However, it omits waves that might be guided in the ionospheric F-layer and ignores lateral variations in the earth's conductivity.

The ionosphere is found to influence the signal by causing its range dependence to change from inverse cube to inverse square beyond about 50 km. That result increases the maximum range predicted for ULF near-field communication systems. The assumption of a resistive layer in the earth between the overburden and the mantle slightly reduces the magnitude of the calculated fields. The layer's primary effect is to reduce the effective ground conductivity seen by surface terminals rather than to support a strong down-under-up signal. None of our calculations predicts that magnetic intensity attenuates as slowly as measured for signals 117 km from a ULF transmitter on the Olympic Peninsula. Analysis of the strong field measured at that site probably requires a more complicated model that includes an ionospheric duct or lateral variations in ground conductivity.

PREFACE

This report develops a theoretical means for predicting ULF near fields at long ranges and, therefore, the maximum range of ULF communication links. Formulas are derived using a five-layer, stratified model of the earth-air-ionosphere system. The model assumes a conductive ionosphere 50 km above a three-layer earth, where a resistive layer is sandwiched between two conductive layers. The results are applicable to the use of ultra-low frequencies for special-purpose communications beyond 100 km, and are of special interest to the U.S. Navy.

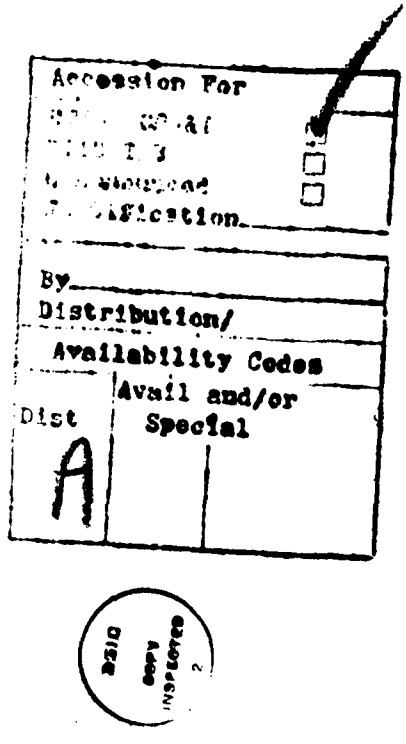

SUMMARY

This report derives formulas for ULF near fields using a five-layer, stratified model of the earth-air-ionosphere system, and gives numerical results for a frequency of 0.1 Hz and ranges between 5 km and 5 Mm. It assumes a semi-infinite, finitely conducting ionosphere 50 km above a three-layer earth, comprising a moderately conductive overburden, a resistive layer, and a highly conductive mantle. It therefore accommodates the two-dimensional confinement of the fields between the earth and the ionosphere as well as possible waveguide modes in the resistive layer. However, it omits waves that might be guided in the ionospheric F-layer and ignores lateral variations in the earth's conductivity.

The ionosphere is found to influence the signal by causing its range dependence to change from inverse cube to inverse square beyond about 50 km. That result increases the maximum range predicted for ULF near-field communication systems. The assumption of a resistive layer in the earth between the overburden and the mantle slightly reduces the magnitude of the calculated fields. The layer's primary effect is to reduce the effective ground conductivity seen by surface terminals rather than to support a strong down-under-up signal. None of our calculations predicts that magnetic intensity attenuates as slowly as measured for signals 117 km from a ULF transmitter on the Olympic Peninsula. Analysis of the strong field measured at that site probably requires a more complicated model that includes an ionospheric duct or lateral variations in ground conductivity.

CONTENTS

FIGURES

I. INTRODUCTION

Research on the terrestrial propagation of long electromagnetic waves has concentrated on low frequencies (LF, 30 to 300 kHz), very low frequencies (VLF, 3 to 30 kHz), and extremely low frequencies (ELF, 30 to 300 Hz), which are commonly used for long-range communication and navigation. Recently, however, the U.S. Navy has become interested in using ultra-low frequencies (ULF, <5 Hz in this report) for special-purpose communications beyond 100 km. At such distances, the ionosphere and the earth's structure must be considered. Moreover, ULF wavelengths are so great that all points on earth are within the near field of aboveground sources. No near-field theory has yet been developed that simultaneously accounts for both the ionosphere and possible resistive layers underground. This report develops a theoretical means for predicting ULF near fields at long ranges and, therefore, the maximum range of ULF communication links.

Even at ELF, transmission distances are usually longer than the inverse wave number, $\lambda/2\pi$ (where λ is the wavelength); thus, the received signal is dominated by the radiation field, which can be represented as modes that propagate in the earth-ionosphere waveguide. Since the opposite is true below 5 Hz, ULF near fields have usually been calculated using the so-called quasi-static theory, which assumes the earth to be a uniform, semi-infinite half space and ignores the ionosphere [Kraichman, 1970]. Two recent analyses have presented double-layer models that more accurately represent the ULF propagation environment. Fraser-Smith and Bubenik [1980] used a model in which a sea of finite depth is bounded below by a uniform earth; and Bannister [1980] developed a two-layer model of the earth. Previous quasi-static models work well if the source and receiver are separated by less than, say, 50 km--the nominal height of the earth-ionosphere waveguide at ULF. However, an even more detailed model is needed to predict propagation at the longer ranges considered here.

One would expect the ionosphere to enhance ULF fields at long distances by causing two-dimensional geometric spreading, rather than

the three-dimensional spreading predicted above a conducting half space. Moreover, a resistive subsurface layer bounded by two conducting layers could enhance ULF fields by supporting down-under-up waveguide modes that attenuate more slowly than near fields. Those possibilities are supported by both theory and experiment. Greifinger and Greifinger [1974] assumed a uniform earth and ionosphere to calculate ULF fields at distances large relative to the height of the earth-ionosphere waveguide. They found an inverse-square dependence on range, instead of the inverse-cube dependence that occurs at short ranges. Bostick, Smith, and Boehl [1977] measured ULF fields at distances up to 117 km from a grounded horizontal-electric-dipole (HED) transmitter and found them to be stronger than predicted by an inverse-cube dependence on range.

This report derives formulas for ULF fields using a five-layer, stratified model of the earth-air-ionosphere system, and gives numerical results for a frequency of 0.1 Hz and ranges between 5 km and 5 Mm. It assumes a semi-infinite, finitely conducting ionosphere 50 km above a three-layer earth, comprising a moderately conductive overburden, a resistive layer, and a highly conductive mantle. It therefore accommodates the two-dimensional confinement of the fields between the earth and the ionosphere as well as possible waveguide modes in the resistive layer. However, it omits waves that might be guided in the ionospheric F-layer [Greifinger and Greifinger, 1968] and ignores lateral variations in the earth's conductivity.

II. ULF SIGNALS MEASURED AT LONG DISTANCES FROM CONTROLLED SOURCE

In 1976, a team of scientists from Pacific-Sierra Research Corporation, the University of Texas, and the Scripps Institution of Oceanography performed an electromagnetic propagation experiment on the Olympic Peninsula in northwest Washington. The experiment was designed to send ULF signals from a land-based transmitter to a receiver on the seafloor [Bostick, Cox, and Field, 1978], but supplementary data were also obtained on land, east of the transmitter, at various distances equal to or greater than the height of the earth-ionosphere waveguide. To our knowledge, these are the only such measurements ever made using a carefully controlled source. The landside data have been reduced but not yet widely distributed [Bostick, Smith, and Boehl, 1977].

This section summarizes the landside data, which contain valuable information on the structure of ULF signals and the media in which they propagate. Although specific to the geophysical conditions at the measurement site, the data clarify the effects of geology on ULF signals and can be used to determine the validity of theoretical models. The landside data comprise magnetotelluric (MT) soundings at many sites on the Olympic Peninsula, and electromagnetic field strengths at distances up to 117 km from a ULF transmitter that operated at square-wave periods between 0.5 and 10 sec. The transmitter was a grounded HED of length L = 1.6 km and current I = 62.4 A at the fundamental frequency.

Figure 1 shows resistivity contours inferred from the MT soundings. Resistivity is seen to depend strongly on depth and range.

Figure 2 shows the magnetic field strengths at a fundamental frequency of 0.1 Hz (dots in error bars) for four distances that exceed the nominal waveguide height of 50 km. It also shows curves that illustrate three range dependences. The solid curve plots the field produced by a grounded HED on a uniform, plane earth. Calculated with the standard quasi-static formula [Kraichman, 1970] for

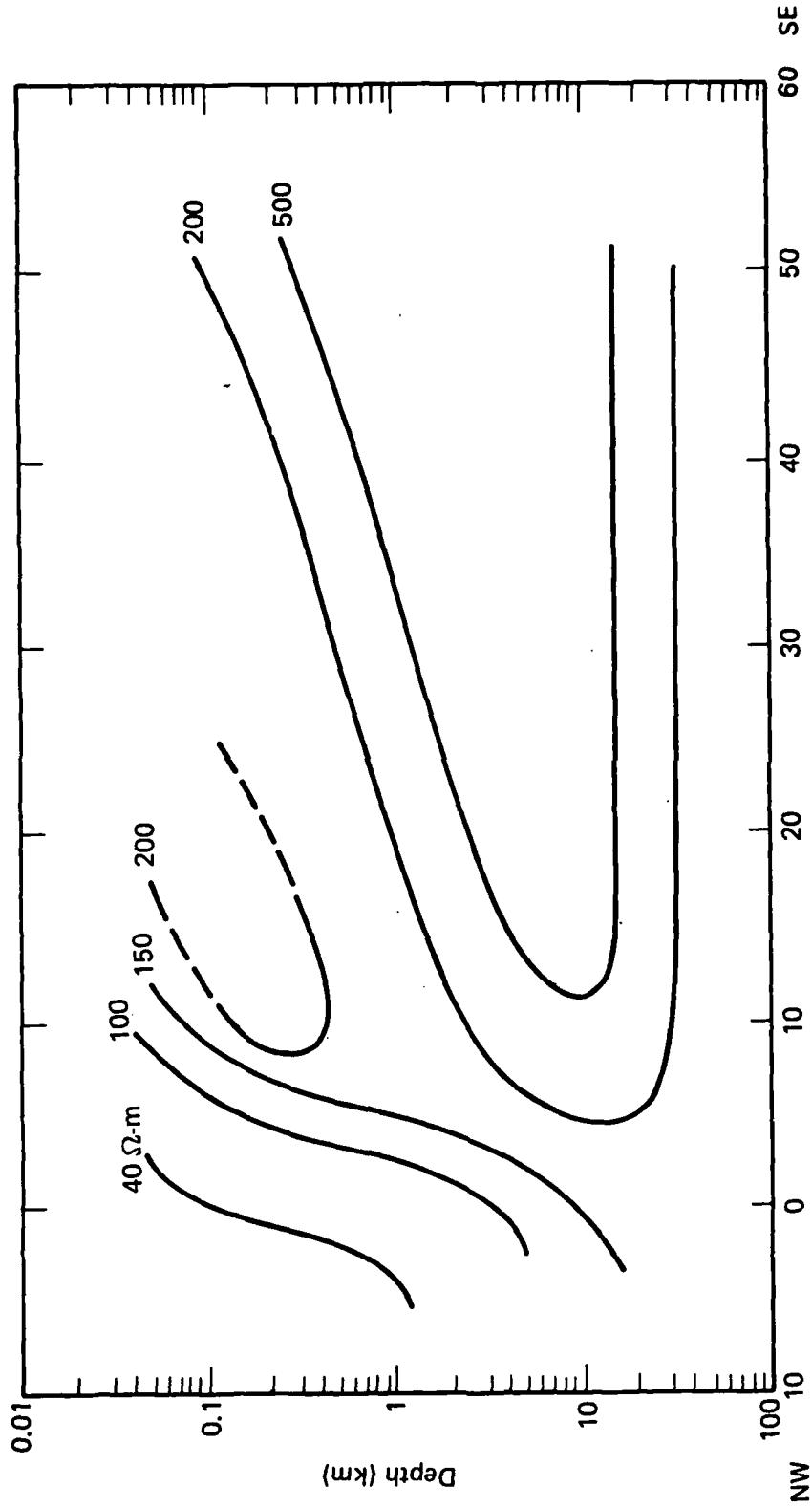

Fig. 1--Transverse section of estimated true resistivity on Olympic Peninsula

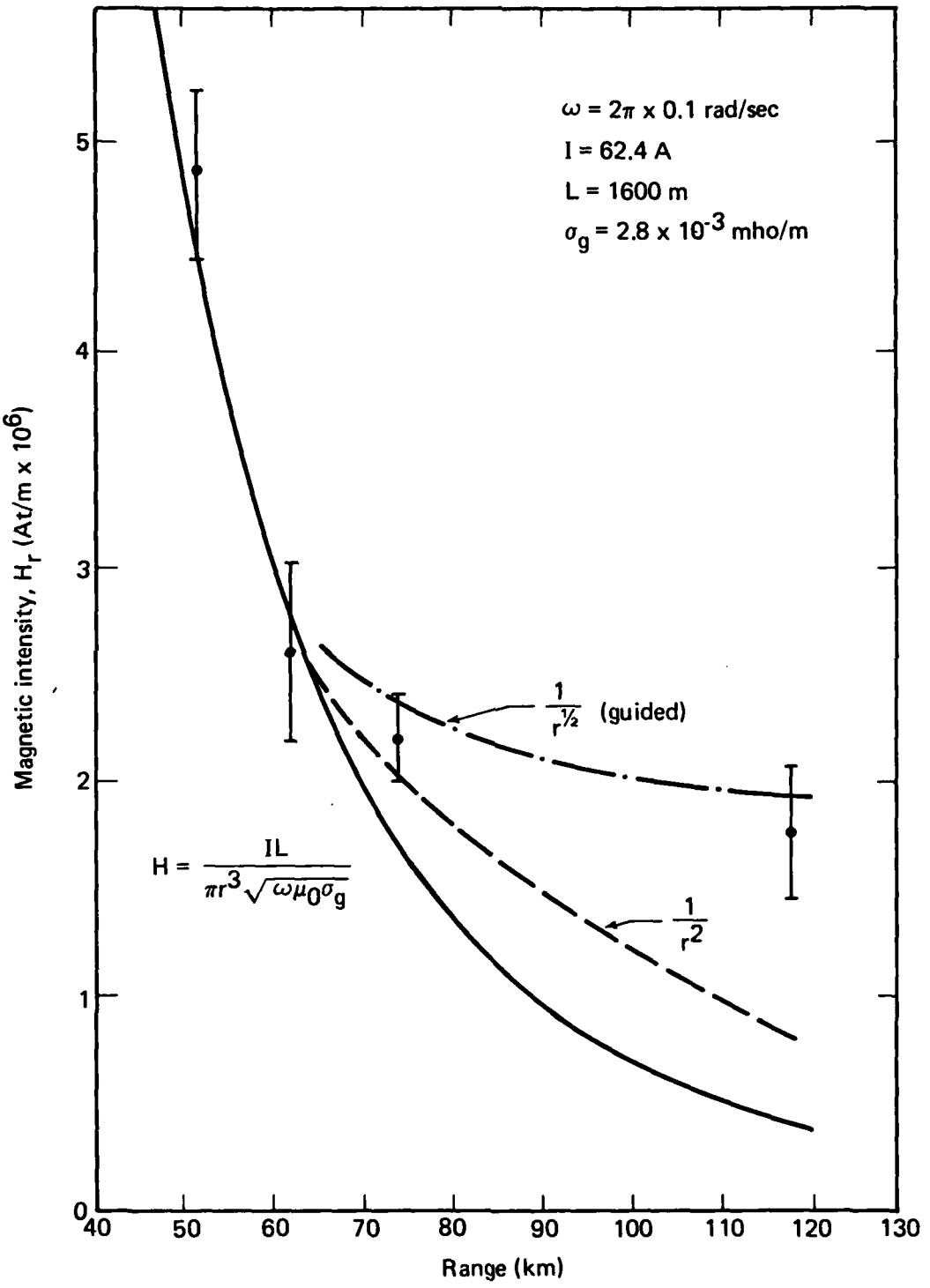

Fig. 2--Measured magnetic intensity versus range

an assumed effective ground conductivity σ_g of 2.8×10^{-3} mho/m, the solid curve agrees with the measurements at ranges up to 60 km, but predicts too small a field at greater ranges. The two other curves, included for comparison, illustrate assumed range dependences. The dashed curve assumes an inverse-square falloff with distance beyond about 60 km, where the ionosphere should cause a transition from three-dimensional to two-dimensional near-field spreading. The dot-and-dash curve assumes an inverse-square-root dependence beyond about 60 km, which would be expected if the wave were guided in the lithosphere or the ionosphere.

III. MATHEMATICAL MODEL

This section summarizes our method for calculating ULF fields. The complicated equations are derived in the Appendix, which also outlines our numerical algorithm.

Figure 3 shows our propagation model, which represents the earth-air-ionosphere system as five layers. Our model reflects many salient features of propagation, including confinement of fields between the earth and the ionosphere, and guidance of waves in a resistive lithospheric layer bounded by an overburden and a mantle, both conductive. By adjusting the widths and conductivities of the layers, we can determine the sensitivity of the fields to the various strata.

Since our model assumes a uniform ionosphere, it must neglect Alfvén waves that might be ducted in the F-layer [Greifinger and Greifinger, 1968]. However, inclusion of such an ionospheric layer would be straightforward. The model also omits the effects of lateral variations in conductivity. The importance of such variations depends strongly on the location of the propagation path. Figure 1 shows substantial lateral variation on the Olympic Peninsula, so our propagation model might be better suited to locations other than the site of the measurements described in Sec. II.

The most common ULF transmitting antenna is a grounded horizontal wire. Such an antenna can be represented as a vertical loop comprising the conductor current in the wire and the return current in the earth. Thus, we assume a horizontal magnetic dipole (HMD) of moment M oriented along the x-axis and centered at a depth d, which is half the effective depth of the return current. The depth d depends on the dipole length L and the effective skin depth in the earth δ_g, but is never greater than $\delta_g/2^{3/2}$.

The general equations in the Appendix are too complicated to solve analytically. However, we obtain useful approximate solutions by further assuming the ionosphere to be perfectly conducting and the earth to be uniform. Specifically, the Appendix shows that, if conductivity

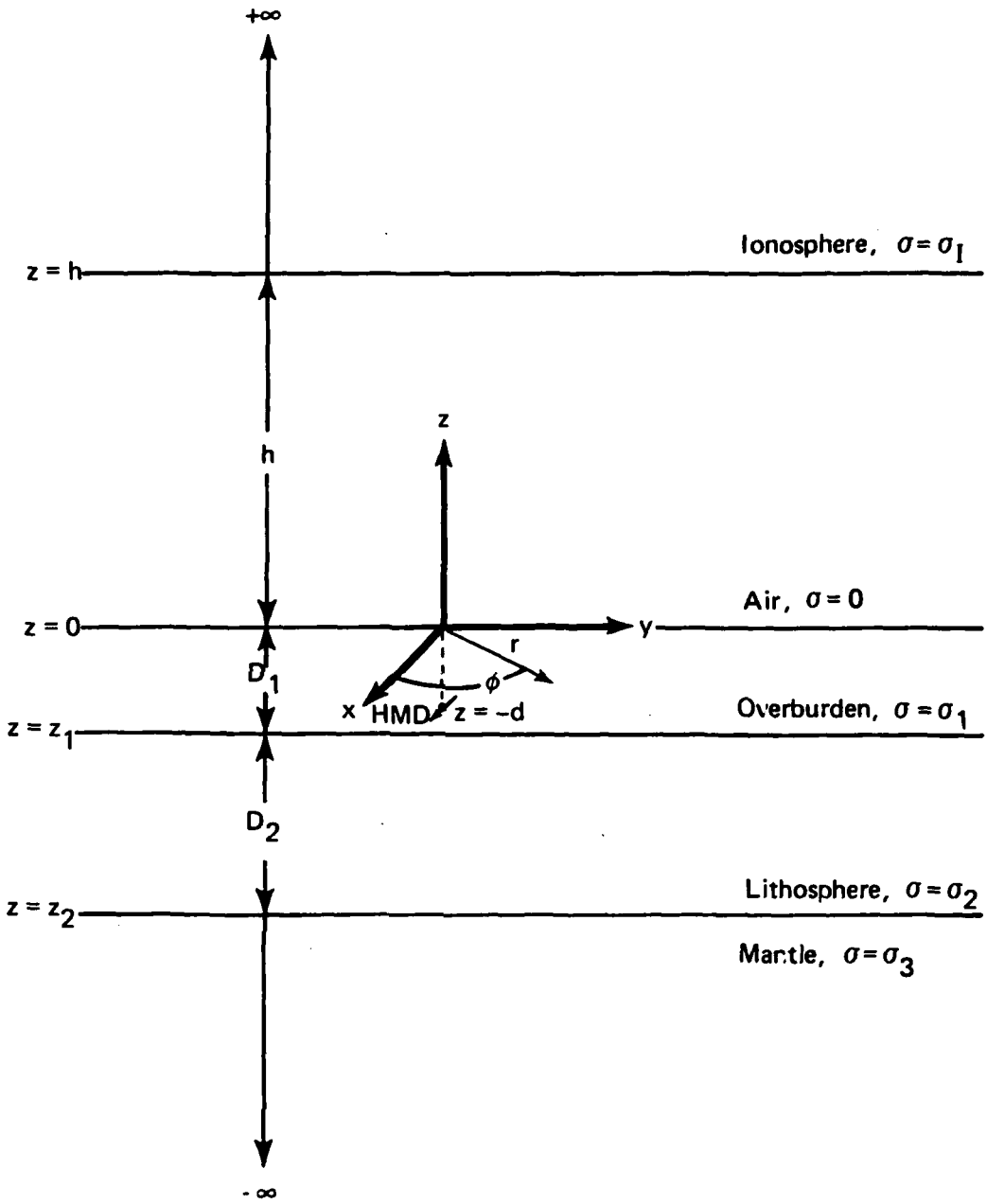

Fig. 3--Model of five-layer, stratified propagation medium

$\sigma_I = \infty$ and distance $D_1 = \infty$, the following simple expressions give the radial magnetic intensity H_r at distances much shorter or greater than the ionospheric height h:*

$$H_r \approx \frac{M}{2\pi r^3} \cos\phi \quad \text{At/m} , \qquad r << h,\ r << \delta_1 , \tag{1}$$

$$H_r \approx \frac{M}{\pi r^3} \cos\phi \quad \text{At/m} , \qquad \delta_1 << r << h , \tag{2}$$

$$H_r \approx \frac{M}{2\pi h r^2} \cos\phi \quad \text{At/m} , \qquad r >> h >> \delta_1 . \tag{3}$$

Using $M = IL\delta_1/\sqrt{2}$ makes Eqs. (1) and (2) equivalent to the standard quasi-static formulas for an HED above a conducting half space. That equivalence is expected, because the effect of the ionosphere is small for ground-level fields when $r << h$. On the other hand, Eq. (3) shows that the near field spreads two-dimensionally ($1/r^2$) rather than three-dimensionally ($1/r^3$) when $r >> h$. Again, that result is expected, because at great distances the source plus its images in the ionosphere and earth behave as an infinitely long line of sources.

Equations (2) and (3) can be combined to obtain the following heuristic formula, which is accurate if $r << h$ or $r >> h$, and works moderately well if $r \approx h$:

$$H_r \approx \frac{M \cos\phi}{2\pi r^2}\left(\frac{r + 2h}{rh}\right) \quad \text{At/m} , \qquad r >> \delta_1 . \tag{4}$$

---

*The coordinate system and many of the geometric symbols are defined in Fig. 3.

IV. NUMERICAL RESULTS

This section presents graphs of the radial magnetic intensity H_r calculated numerically from equations given in the Appendix. We can easily compute the other field components from equations also given in the Appendix, but, for brevity, omit them.

All calculations assume $M = 4\pi$ A-m^2 and $\cos \phi = 1$; distances are expressed in kilometers. The results may be scaled to any situation by multiplying them by the factor

$$\frac{M \cos \phi}{4\pi} \times 10^{-9} , \tag{5}$$

where M is the actual HMD moment expressed in units of ampere meters squared. To compare the graphs in this section with the measured fields shown in Fig. 2, use $M = 2 \times 10^9$ A-m^2 in the conversion factor (5). The effective HMD moment created by a grounded HED varies as $1/\sqrt{f\sigma_g}$, where f is the frequency. Therefore, holding M constant at 4π A-m^2 does not necessarily correspond to holding IL constant.

PERFECTLY CONDUCTING EARTH AND IONOSPHERE

Figure 4 shows H_r as a function of distance for the idealized case where the earth and ionosphere are assumed to be perfectly conducting, semi-infinite half spaces separated by 50 km. For comparison, the figure also shows H_r as calculated from the heuristic Eq. (4). The transition from an inverse-cube to an inverse-square range dependence at $r \approx 2h$ is apparent. The simple formula given by Eq. (4) is accurate if $r << 2h$ or $r >> 2h$, but slightly overestimates the field at $r \approx 2h$.

DEPENDENCE ON GROUND CONDUCTIVITY

To determine the effect of ground conductivity on the field, we calculate H_r for a three-layer model. Formally, we take $D_1 = \infty$ and $\sigma_1 = \sigma_g$ (see Fig. 3), and vary σ_g parametrically while holding the

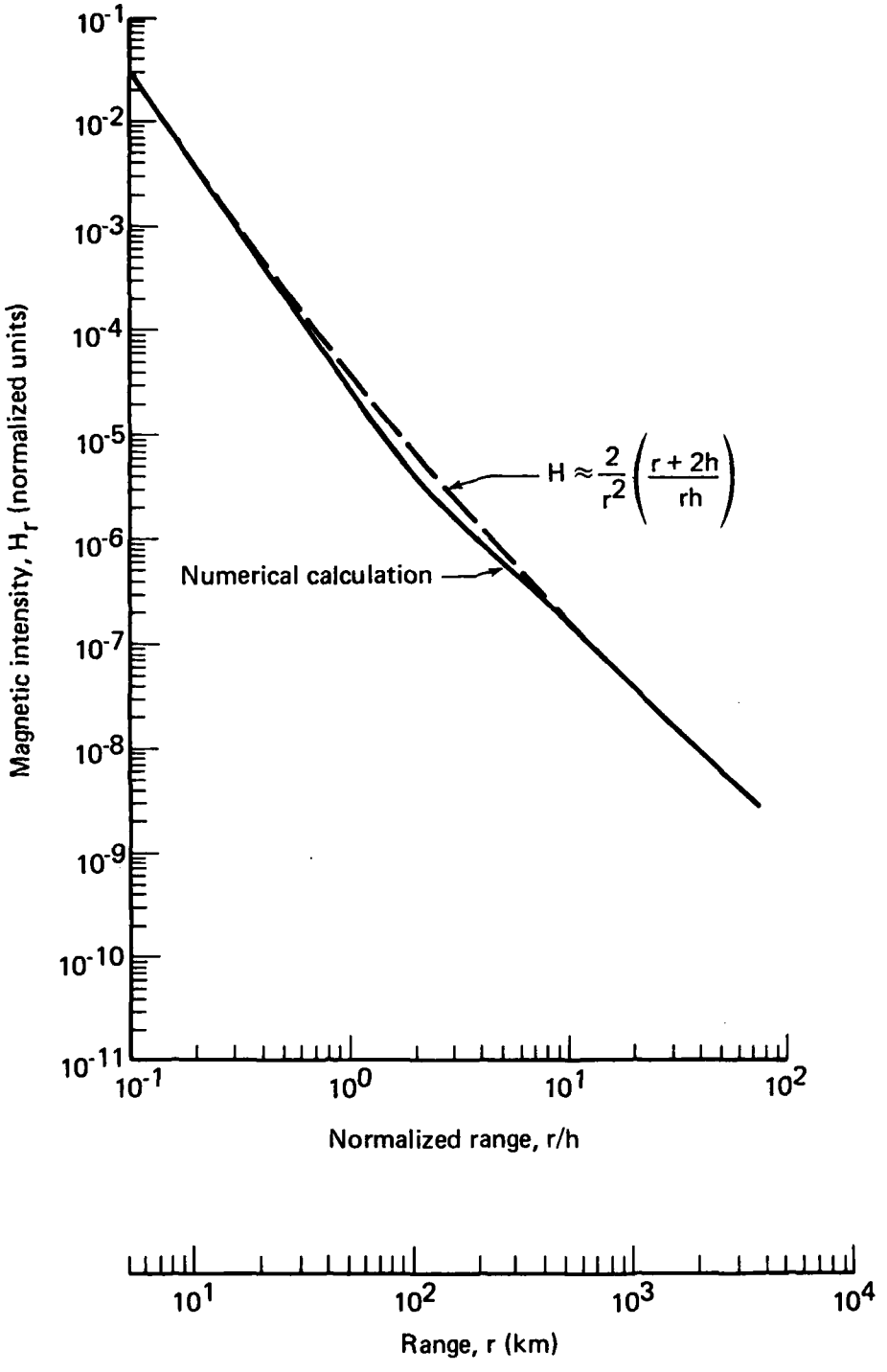

Fig. 4--Calculated magnetic intensity versus range for perfectly conducting earth and ionosphere and f = 0.1 Hz

effective ionospheric conductivity σ_I constant. Figures 5 through 8 show a series of such calculations made for $\sigma_I = 10^{-2}$, 10^{-3}, 10^{-4}, and 10^{-5} mho/m, respectively. It is difficult to assign a precise value to σ_I because ULF waves interact with the ionosphere over a broad range of altitudes. The four values used in our calculations span reasonable averages over a broad altitude range, with $\sigma_I \approx 10^{-3}$ to 10^{-4} mho/m perhaps representing the best estimates for daytime.

Figure 5 shows that, at long ranges, the field depends strongly on effective ground conductivity σ_g if the effective conductivity of the ionosphere is high ($\sigma_I = 10^{-2}$ mho/m). If r exceeds 100 km, H_r is an order of magnitude greater for $\sigma_g = 0.1$ mho/m than for $\sigma_g = 10^{-4}$ mho/m. However, as shown by Figs. 6 through 8, the effect of ground conductivity on H_r diminishes as σ_I becomes smaller. Figure 8 shows that H_r is nearly independent of ground conductivity if $\sigma_I = 10^{-5}$ mho/m.

Figures 9 through 12 show the dependence of H_r on σ_I for $\sigma_g = 10^{-1}$, 10^{-2}, 10^{-3}, and 10^{-4} mho/m, respectively. The long-range signal depends strongly on σ_I if the effective ground conductivity is high (Fig. 9), and weakly on σ_I if the effective ground conductivity is low (Fig. 12).

As expected, Figs. 5 through 12 show that the signal is degraded by imperfect ground or ionospheric conductivity. In all cases, however, the long-range signal is stronger than predicted by the standard quasi-static formula, which neglects the ionosphere by assuming $\sigma_I = 0$.

To evaluate the possible effect of a lithospheric waveguide on the ground-level signal, we have calculated H_r for the five-layer model, using several assumed values for the conductivity σ_2 of the lithospheric layer. Such a resistive layer could affect the signal strength in two competing ways. First, it could enhance the long-range signal by supporting waveguide modes that decrease more slowly with distance than does the aboveground near field. Second, it could degrade the signal by reducing the effective ground conductivity seen by surface terminals.

Figure 13 plots H_r calculated for a 5 km resistive layer between a 1 km overburden of conductivity 10^{-2} mho/m and a mantle of conductivity 1 mho/m--a high value. This model, which also includes an

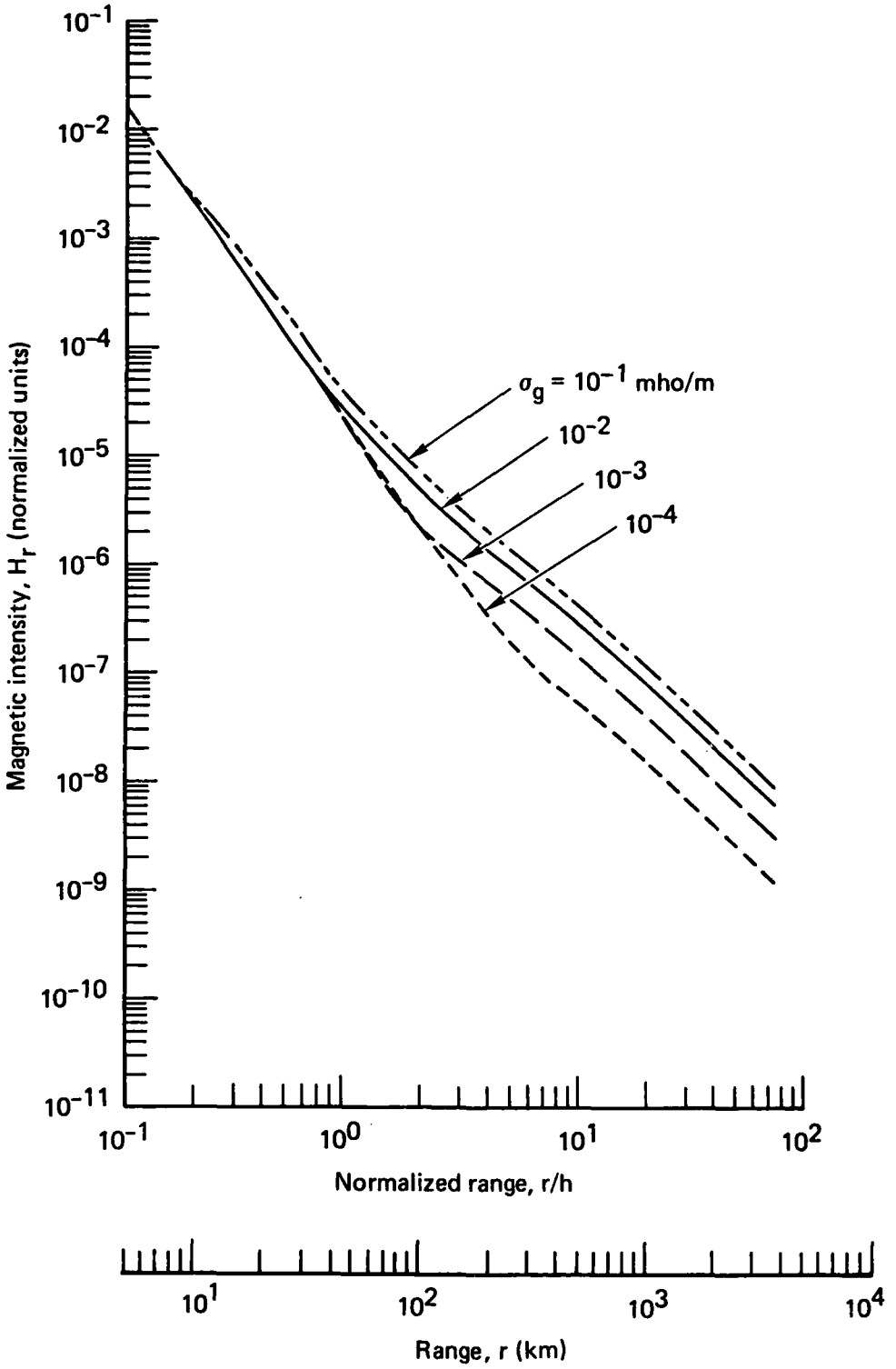

Fig. 5--Calculated magnetic intensity versus range and effective ground conductivity σ_g for $\sigma_I = 10^{-2}$ mho/m and f = 0.1 Hz

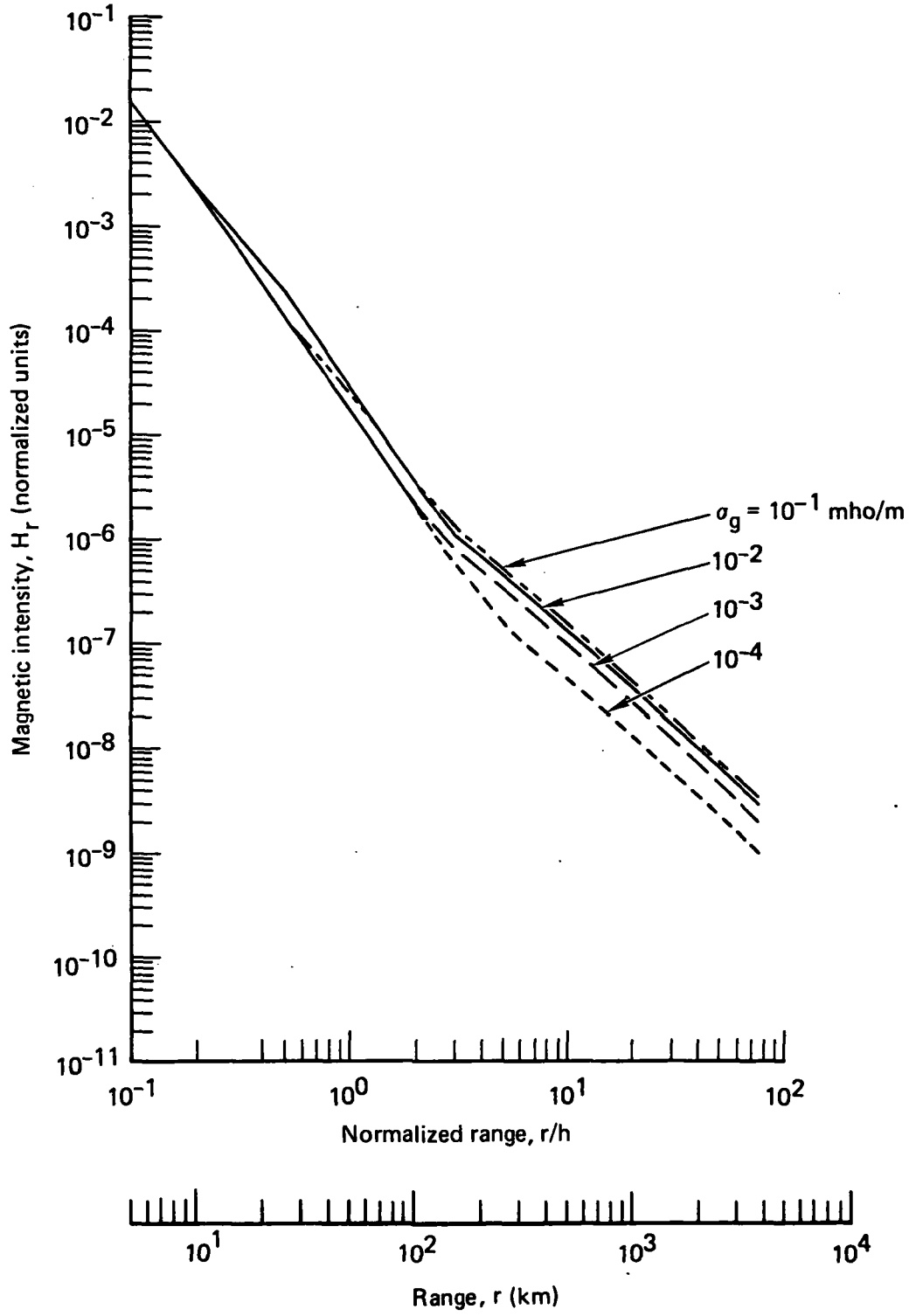

Fig. 6--Calculated magnetic intensity versus range and effective ground conductivity σ_g for $\sigma_I = 10^{-3}$ mho/m and f = 0.1 Hz

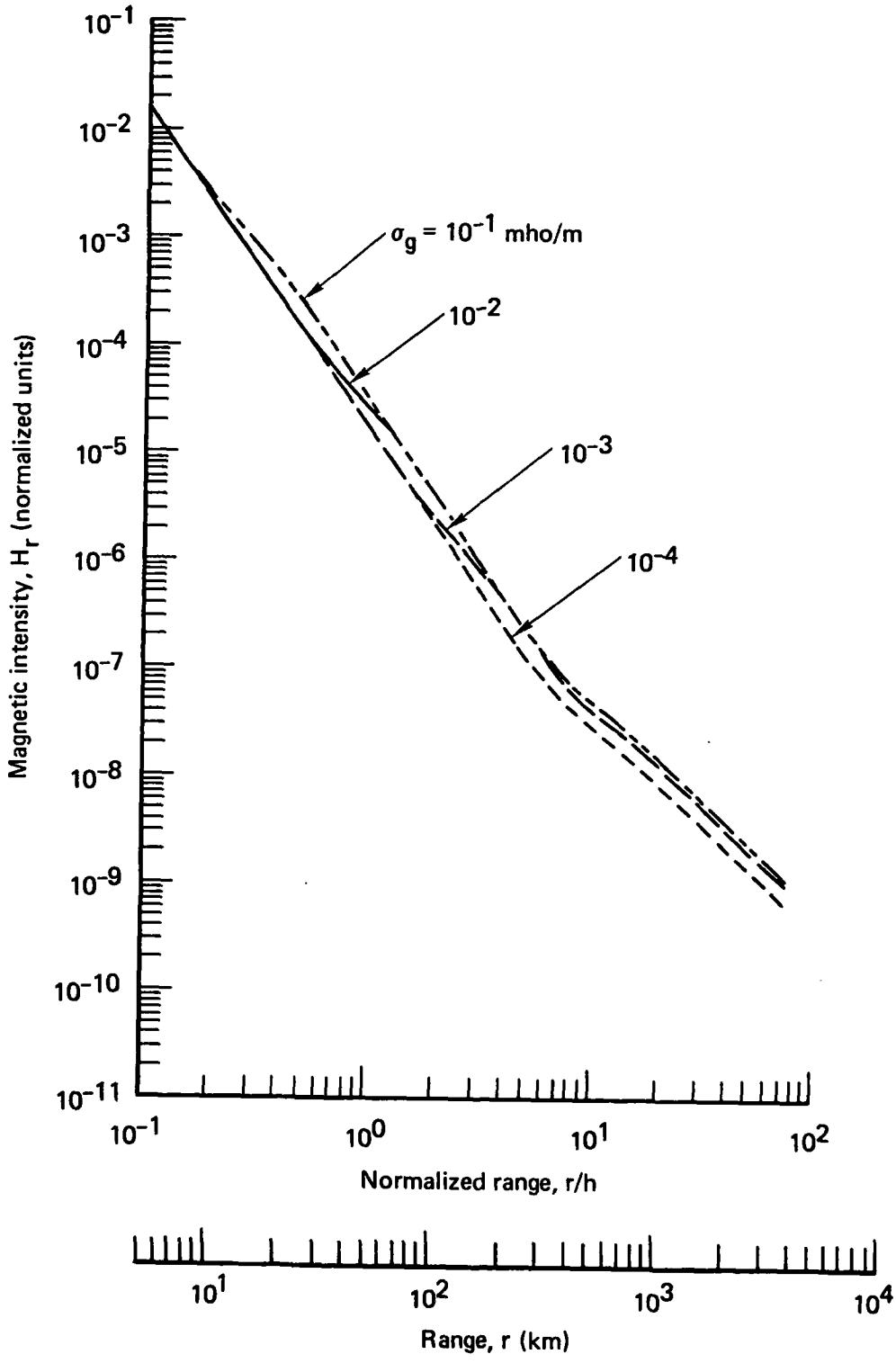

Fig. 7--Calculated magnetic intensity versus range and effective ground conductivity σ_g for $\sigma_I = 10^{-4}$ mho/m and f = 0.1 Hz

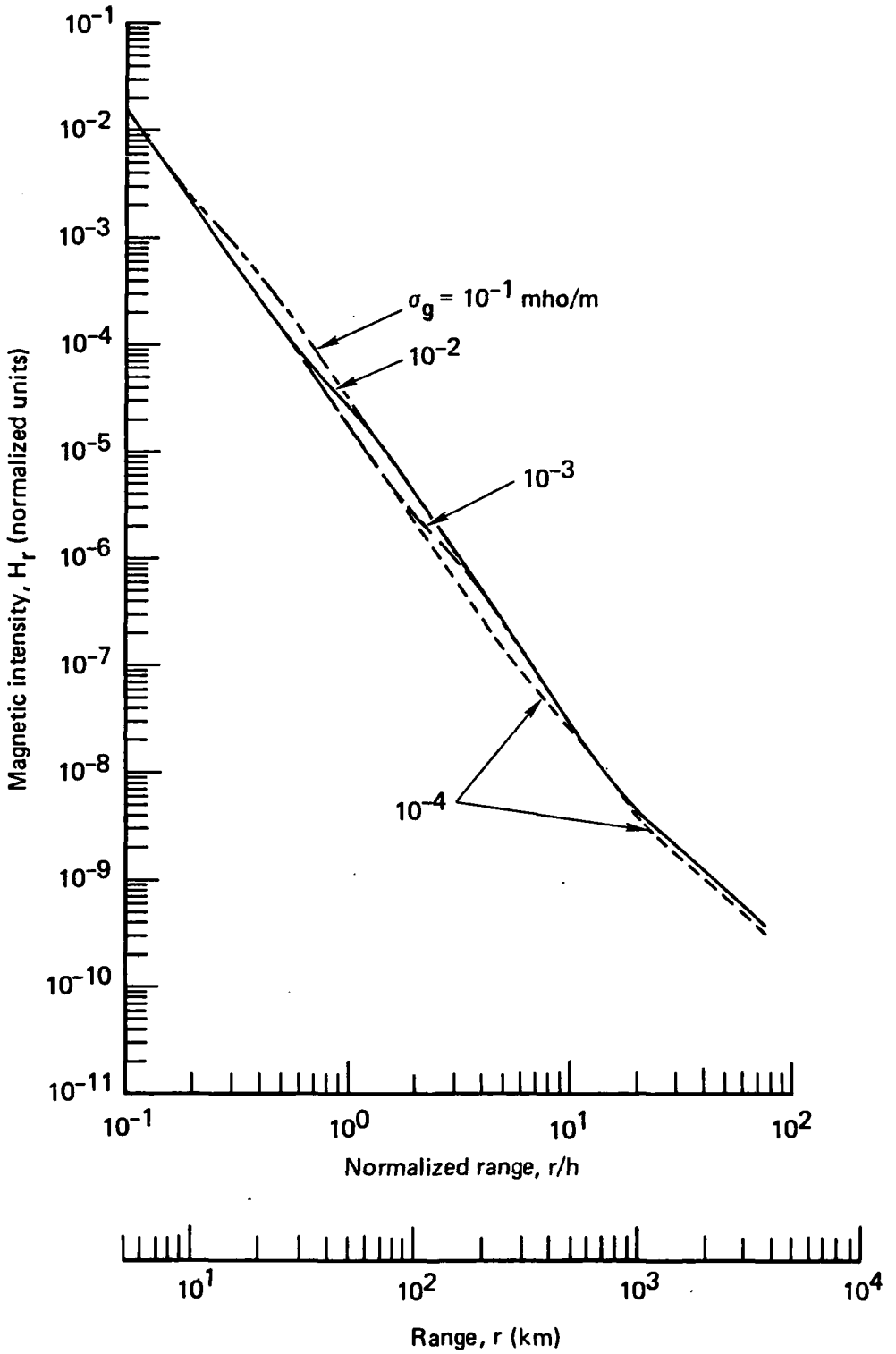

Fig. 8--Calculated magnetic intensity versus range and effective ground conductivity σ_g for $\sigma_I = 10^{-5}$ mho/m and f = 0.1 Hz

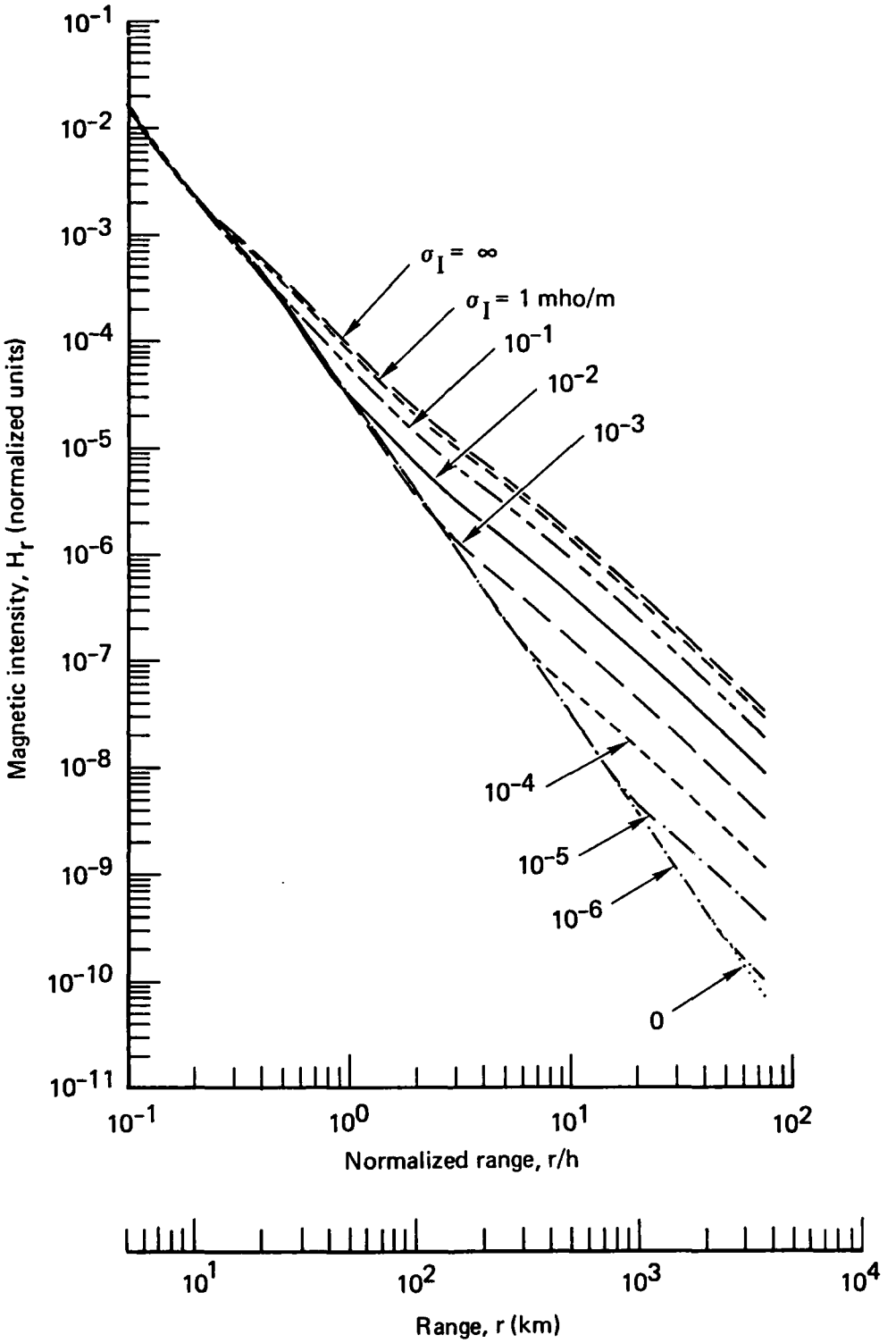

Fig. 9--Calculated magnetic intensity versus range and effective ionospheric conductivity σ_I for $\sigma_g = 10^{-1}$ mho/m and f = 0.1 Hz

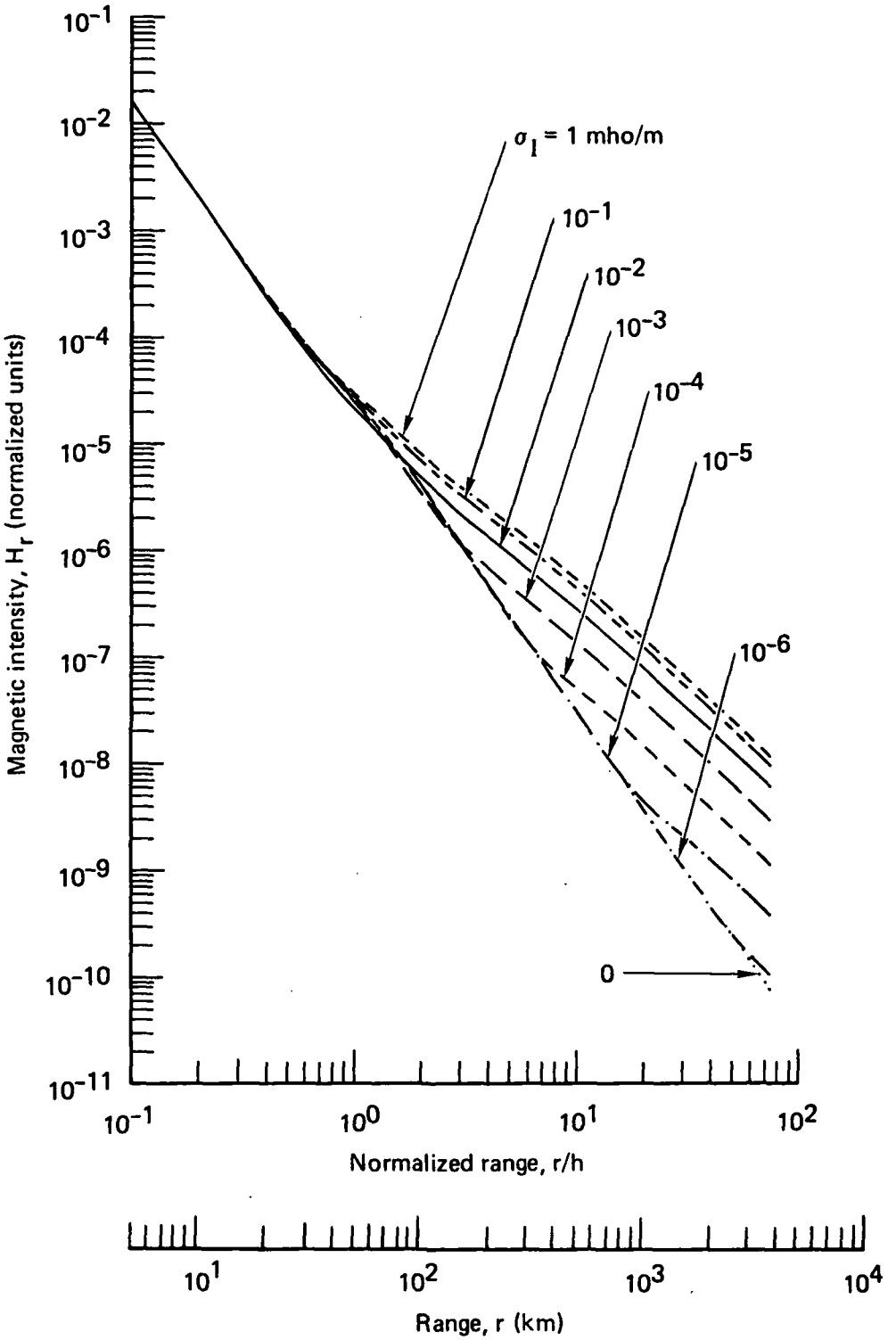

Fig. 10--Calculated magnetic intensity versus range and effective ionospheric conductivity σ_I for $\sigma_g = 10^{-2}$ mho/m and f = 0.1 Hz

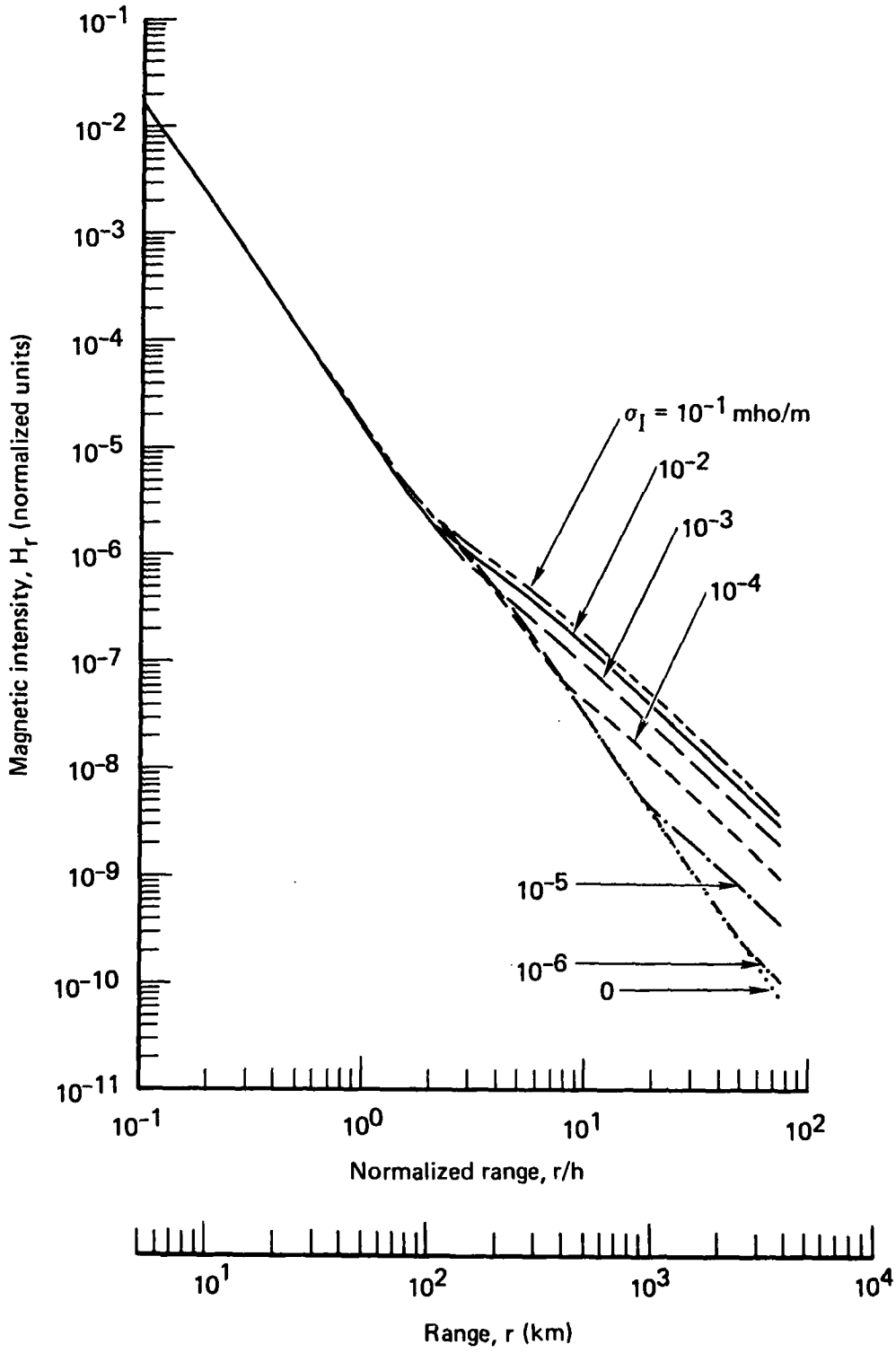

Fig. 11--Calculated magnetic intensity versus range and effective ionospheric conductivity σ_I for $\sigma_g = 10^{-3}$ mho/m and f = 0.1 Hz

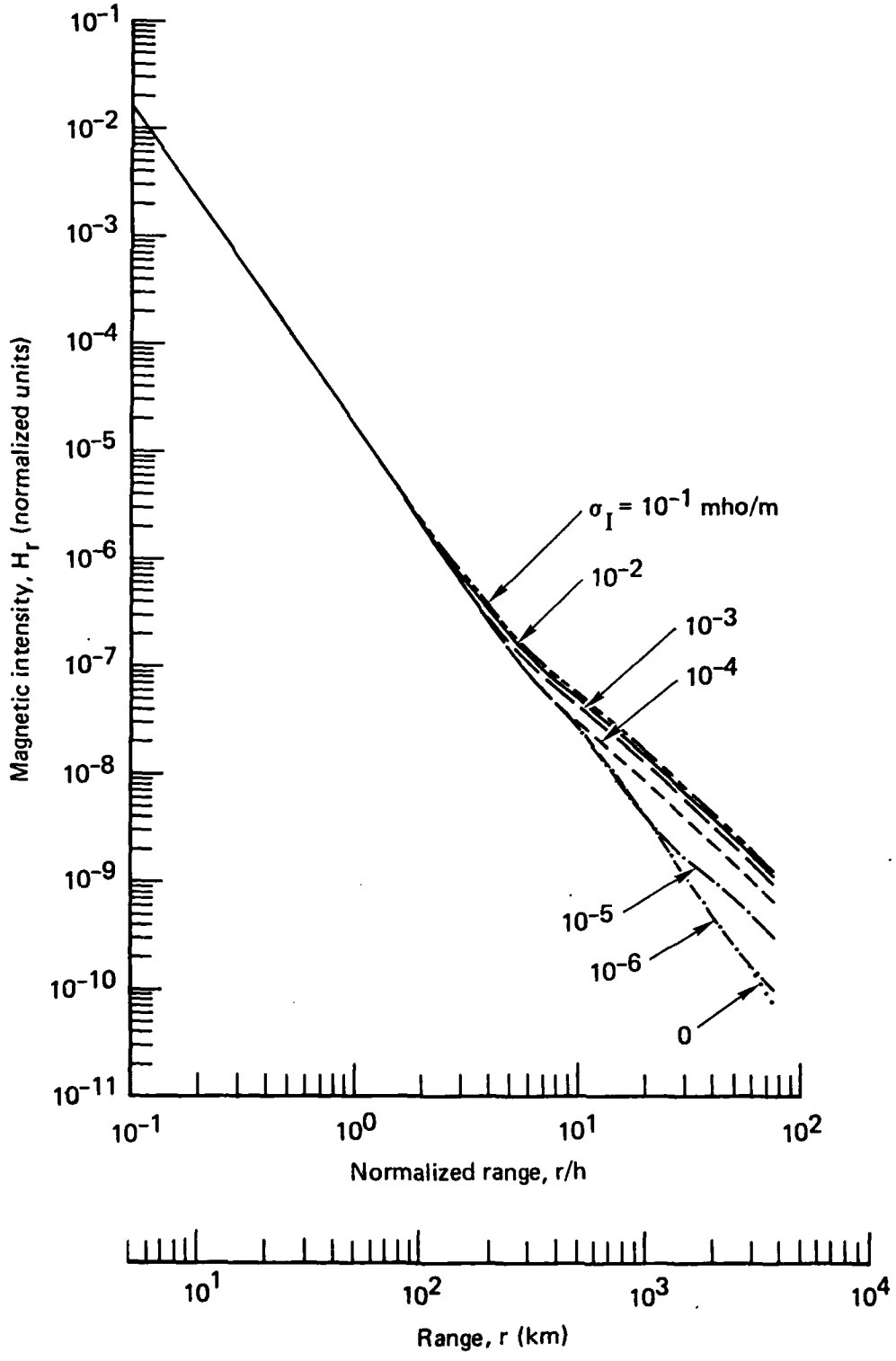

Fig. 12--Calculated magnetic intensity versus range and effective ionospheric conductivity σ_I for $\sigma_g = 10^{-4}$ mho/m and f = 0.1 Hz

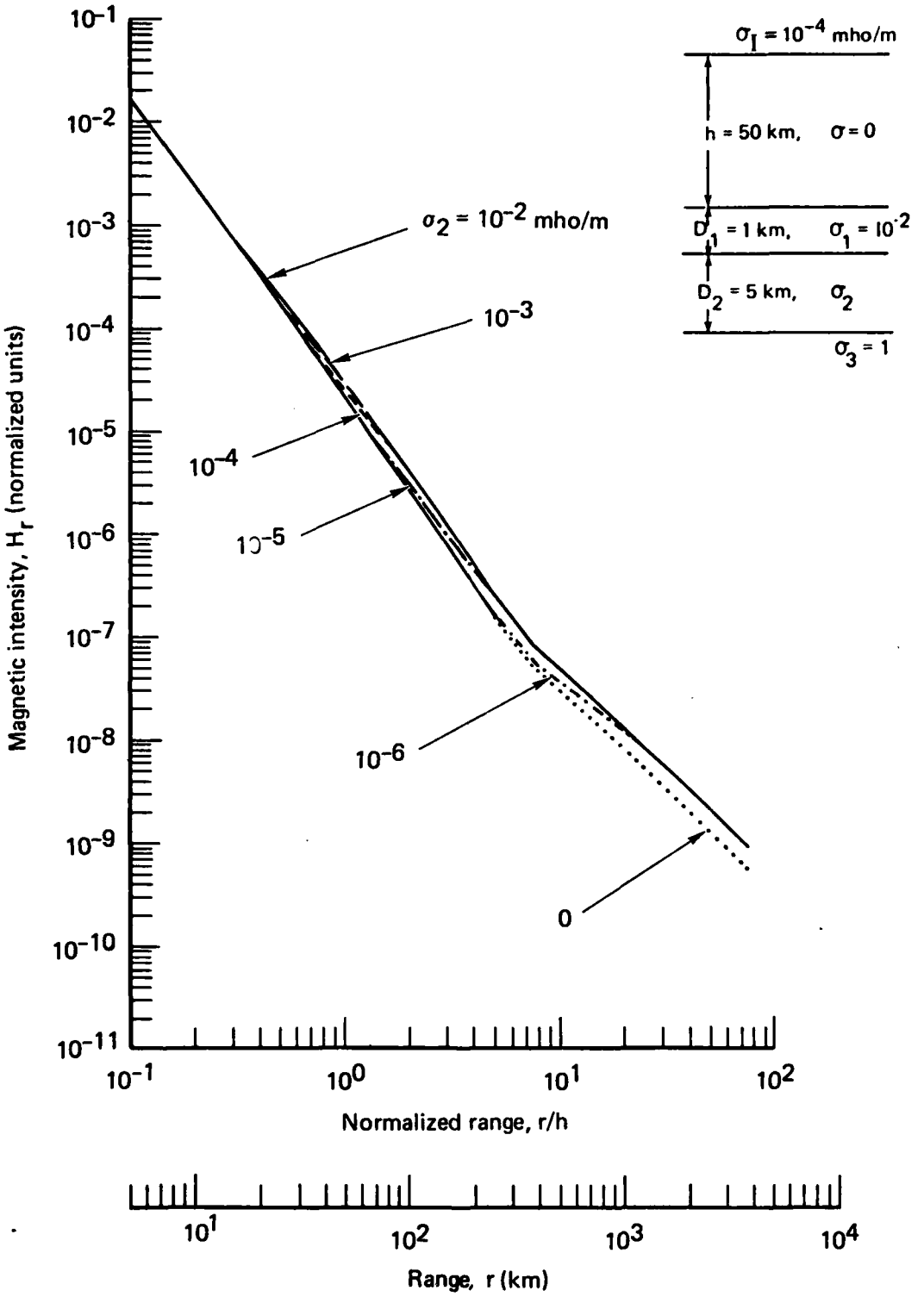

Fig. 13--Calculated magnetic intensity versus range for various values of lithospheric conductivity σ_2, a layer width of 5 km, and f = 0.1 Hz

ionosphere of effective conductivity $\sigma_I = 10^{-4}$ mho/m, is sketched in the insert to the figure. The results show that H_r is insensitive to the conductivity of the resistive layer. Calculations performed for other values of σ_1, D_1, and D_2 indicate similarity to the representative behavior illustrated in Fig. 13.

In all cases considered, the resistive layer slightly weakened the signal at long ranges, compared with that for a uniform earth. Thus, the primary consequence of the layer is to reduce the effective ground conductivity rather than to enhance the field through a down-under-up propagation mode.

V. CONCLUSIONS

In calculating the effect of a uniform ionosphere and a three-layer, stratified earth on the range dependence of ground-level ULF near fields, we found that the ionosphere strongly influences the signal by causing its range dependence to change from inverse cube to inverse square beyond about 50 km. Thus, long-range ULF signals are much stronger than indicated by the standard quasi-static formulas, which apply only to ranges shorter than 50 km and predict that the magnetic intensity decreases as the inverse cube of range. That result increases the maximum range predicted for ULF near-field communication systems.

The assumption of a resistive layer in the earth between the overburden and the mantle slightly reduces the magnitude of the calculated fields. The layer's primary consequence is to reduce the effective ground conductivity seen by surface terminals rather than to support a strong down-under-up signal.

None of our calculations predicts that magnetic intensity attenuates as slowly as measured for signals 117 km from a ULF transmitter on the Olympic Peninsula. Analysis of the strong measured field probably requires a more complicated model that includes an ionospheric duct or lateral variations in ground conductivity.

Appendix

DERIVATION OF EQUATIONS

This appendix derives the equations that describe the electromagnetic fields on the surface of the earth, which is represented in three layers by the model in Fig. 3 (p. 8).

GENERAL EQUATIONS

We begin by defining the Hertz potential $\vec{\pi}$ as

$$\vec{H} = k^2\vec{\pi} + \vec{\nabla}(\vec{\nabla} \cdot \vec{\pi}) \tag{A.1}$$

and

$$\vec{E} = -i\omega\mu\, \vec{\nabla} \times \vec{\pi} \ , \tag{A.2}$$

where $\vec{H}$ and $\vec{E}$ are the magnetic and electric fields, respectively, the complex propagation constant $k^2 = \omega^2\mu_0\varepsilon - i\omega\mu_0\sigma$, and the complex refractive index n^2 is

$$n^2 = \varepsilon + \frac{\sigma}{i\omega} \ . \tag{A.3}$$

We represent the HED antenna and its ground return current as an HMD of moment $\vec{M}$ centered at a depth d below the earth's surface. Specifically, we write

$$(\nabla^2 + k^2)\vec{\pi} = -\vec{M} \ , \tag{A.4}$$

where

$$\vec{M} = M\delta(x)\delta(y)\delta(z + d)\hat{e}_x \ . \tag{A.5}$$

Here, $\hat{e}_x$ is a unit vector and

$$M = \text{(dipole current)(dipole area)} \ . \tag{A.6}$$

Following Sommerfeld [1949], we write

$$\vec{\pi}_i = \alpha_i \hat{e}_x + \beta_i \hat{e}_y \ , \tag{A.7}$$

where the subscript i denotes the layers (i = I, 0, 1, 2, 3) illustrated in Fig. 3. It can be shown, after considerable rearrangement, that

$$\alpha_i = \frac{M}{4\pi} \int_0^\infty \left[A_i(\lambda)\, e^{\gamma_i z} + B_i(\lambda)\, e^{-\gamma_i z} - S_i(\lambda, z) \right] J_0(\lambda r) \lambda \, d\lambda \tag{A.8}$$

and

$$\beta_i = -\cos\phi \, \frac{M}{4\pi} \int_0^\infty \left[C_i(\lambda)\, e^{\gamma_i z} + D_i(\lambda)\, e^{-\gamma_i z} \right] J_1(\lambda r) \lambda^2 \, d\lambda \ , \tag{A.9}$$

where $\gamma_i^2 = \lambda^2 + k_i^2$, $\mathrm{Re}\,\gamma_i > 0$, and $S_i = 1/\gamma_i \exp(-\gamma_i |z + d|)$ if the dipole is in the layer, and 0 otherwise. The functions A_i, B_i, C_i, and D_i can be found from the radiation condition $\vec{\pi} \to 0$ at $z = \pm\infty$ and the boundary conditions

$$k_i^2 \alpha_i(z_i) = k_{i+1}^2 \alpha_{i+1}(z_i) \ , \tag{A.10}$$

$$\frac{\partial}{\partial z} \alpha_i \Big|_{z=z_i} = \frac{\partial}{\partial z} \alpha_{i+1} \Big|_{z=z_i} \ , \tag{A.11}$$

$$\beta_i(z_i) = \beta_{i+1}(z_i) \ , \tag{A.12}$$

$$\frac{\partial}{\partial z} \beta_i \Big|_{z=z_i} + \frac{\partial \alpha_i}{\partial x} \Big|_{z=z_i} = \frac{\partial}{\partial z} \beta_{i+1} \Big|_{z=z_i} + \frac{\partial \alpha_{i+1}}{\partial x} \Big|_{z=z_i} \ . \tag{A.13}$$

Equations (A.1) through (A.13) can then be used to find the following expressions for the field components at the earth's surface:

$$H_r = -\frac{M}{4\pi}\cos\phi\int_0^\infty F_1(\lambda)\left[J_0(\lambda r)\lambda - \frac{1}{r}J_1(\lambda r)\right]\lambda^2\,d\lambda\ , \qquad (A.14)$$

$$H_\phi = \frac{M}{4\pi}\sin\phi\,\frac{1}{r}\int_0^\infty F_1(\lambda)J_1(\lambda r)\lambda^2\,d\lambda\ , \qquad (A.15)$$

$$H_z = -\frac{M}{4\pi}\cos\phi\int_0^\infty F_2(\lambda)J_1(\lambda r)\lambda^2\,d\lambda\ , \qquad (A.16)$$

$$E_r = i\omega\mu\frac{M}{4\pi}\sin\phi\int_0^\infty \left[F_3(\lambda)J_0(\lambda r) - \frac{1}{r}\lambda F_4(\lambda)J_1(\lambda r)\right]\lambda\,d\lambda\ , \qquad (A.17)$$

$$E_\phi = -i\omega\mu\frac{M}{4\pi}\cos\phi\int_0^\infty \left[F_5(\lambda)J_0(\lambda r)\lambda - \frac{1}{r}F_4(\lambda)J_1(\lambda r)\right]\lambda^2\,d\lambda\ , \qquad (A.18)$$

$$E_z = -i\omega\mu\frac{M}{4\pi}\sin\phi\int_0^\infty F_6(\lambda)J_1(\lambda r)\lambda^2\,d\lambda\ . \qquad (A.19)$$

In Eqs. (A.14) through (A.19), the functions F are given by

$$F_1(\lambda) = A_0 + B_0 + \lambda(C_0 - D_0)\ , \qquad (A.20)$$

$$F_2(\lambda) = [A_0 - B_0 + \lambda(C_0 + D_0)]\lambda\ , \qquad (A.21)$$

$$F_3(\lambda) = \lambda(A_0 - B_0)\ , \qquad (A.22)$$

$$F_4(\lambda) = C_0 + D_0 \ , \tag{A.23}$$

$$F_5(\lambda) = (A_0 - B_0) - (C_0 + D_0)\lambda \ , \tag{A.24}$$

$$F_6(\lambda) = A_0 + B_0 \ . \tag{A.25}$$

Application of the boundary conditions for the model shown in Fig. 3 gives the following expressions for A_0, B_0, C_0, and D_0:

$$A_0 = \frac{2}{\gamma_0} \Phi_A K \, e^{-\gamma_1 d} \ , \tag{A.26}$$

$$B_0 = \frac{2}{\gamma_0} \Phi_B K \, e^{-\gamma_1 d} \ , \tag{A.27}$$

$$\begin{aligned} C_0 = {} & \Big[\Delta_{-1} \, e^{-\gamma_0 h} \Big[\rho_0(\rho_1 + \rho_2') \, e^{-2\gamma_1 D_1} + (1 + \rho_1\rho_2') \Big] \\ & - \rho_{-1}' \Big\{ \Delta_0 \Big[(\rho_1 + \rho_2') \, e^{-2\gamma_1 D_1} + (1 + \rho_1\rho_2') \Big] \\ & + (1 - \rho_0) \, e^{-\gamma_1 D_1} \Big[\Delta_1(1 + \rho_2') + \Delta_2(1 - \rho_1) \, e^{-\gamma_2 D_2} \Big] \Big\} \Big] \\ & \div \Big[(\rho_{-1}' + \rho_0)(\rho_1 + \rho_2') \, e^{-2\gamma_1 D_1} + (\rho_0\rho_{-1}' + 1)(1 + \rho_1\rho_2') \Big] \ , \end{aligned} \tag{A.28}$$

$$\begin{aligned} D_0 = {} & \Big\{ \Delta_{-1} \, e^{-\gamma_0 h} \Big[(\rho_1 + \rho_2') \, e^{-2\gamma_1 D_1} + \rho_0(1 + \rho_1\rho_2') \Big] \\ & + \Delta_0 \Big[(\rho_1 + \rho_2') \, e^{-2\gamma_1 D_1} + (1 + \rho_1\rho_2') \Big] \\ & + (1 - \rho_0) \, e^{-\gamma_1 D_1} \Big[\Delta_1(1 + \rho_2') + \Delta_2(1 - \rho_1) \, e^{-\gamma_2 D_2} \Big] \Big\} \\ & \div \Big[(\rho_{-1}' + \rho_0)(\rho_1 + \rho_2') \, e^{-2\gamma_1 D_1} + (\rho_0\rho_{-1}' + 1)(1 + \rho_1\rho_2') \Big] \ , \end{aligned} \tag{A.29}$$

where

$$\Phi_A = \frac{e^{-2\gamma_0 h}}{e^{-2\gamma_0 h} - 1}, \tag{A.30}$$

$$\Phi_B = \frac{1}{e^{-2\gamma_0 h} - 1}, \tag{A.31}$$

$$K = \frac{1 + e^{-2\gamma_1 (D_1 - d)} \Lambda}{1 + e^{-2\gamma_1 D_1} \Lambda}, \tag{A.32}$$

$$\Lambda = \frac{\tau_1 + \tau_2 e^{-2\gamma_2 D_2}}{1 + \tau_1 \tau_2 e^{-2\gamma_2 D_2}}, \tag{A.33}$$

$$\rho_i = \frac{\gamma_i - \gamma_{i+1}}{\gamma_i + \gamma_{i+1}}, \tag{A.34}$$

$$\tau_i = \frac{\gamma_i k_{i+1}^2 - \gamma_{i+1} k_i^2}{\gamma_i k_{i+1}^2 + \gamma_{i+1} k_i^2}, \tag{A.35}$$

$$\rho'_{-1} = \rho_{-1} e^{-2\gamma_0 h}, \qquad \rho'_2 = \rho_2 e^{-2\gamma_2 D_2}, \tag{A.36}$$

$$\Delta_{-1} = -\frac{2}{\gamma_{-1} + \gamma_0} B_0 e^{-\gamma_0 h}, \tag{A.37}$$

$$\Delta_0 = \frac{1}{\gamma_0 + \gamma_1} B_0 \left(1 + e^{-2\gamma_0 h}\right), \tag{A.38}$$

$$\Delta_1 = \frac{1}{\gamma_1 + \gamma_2}\left[A_1 e^{-\gamma_1 D_1} + B_1 e^{\gamma_1 D_1} - \frac{1}{\gamma_1} e^{-\gamma_1 (D_1 - d)}\right.$$

$$\left. - A_2 e^{-\gamma_2 D_1} (1 + \eta)\right] , \qquad (A.39)$$

$$\Delta_2 = \frac{1}{\gamma_2 + \gamma_3}\left[A_2 e^{-\gamma_2 (D_1 + D_2)} (1 + \tau_2) - A_3 e^{-\gamma_3 (D_1 + D_2)}\right] , \qquad (A.40)$$

$$\eta = \tau_2 e^{-2\gamma_2 D_2} , \qquad (A.41)$$

$$A_1 = \frac{1}{\gamma_1} K e^{-\gamma_1 d} , \qquad (A.42)$$

$$B_1 = \frac{1}{\gamma_1} (1 - K) e^{-\gamma_1 d} , \qquad (A.43)$$

$$A_2 = \frac{\gamma_1}{\gamma_2} e^{\gamma_2 D_1} \frac{1}{1 - \eta}\left[A_1 e^{-\gamma_1 D_1} - B_1 e^{-\gamma_1 D_1} - \frac{1}{\gamma_1} e^{-\gamma_1 (D_1 - d)}\right] , \qquad (A.44)$$

$$A_3 = \frac{\gamma_2}{\gamma_3} e^{\gamma_3 (D_1 + D_2)} (1 - \tau_2) e^{-\gamma_2 (D_1 + D_2)} A_2 . \qquad (A.45)$$

To derive Eqs. (A.26) through (A.45), we assumed $k_0^2 \approx 0$, so $\gamma_0 \approx \lambda$. That assumption constitutes the quasi-static approximation, which is valid anywhere on earth for frequencies below a few hertz. We made this approximation to save computation time. The results presented in Sec. IV show the radial magnetic intensity, computed from Eq. (A.14) using the numerical procedure given below.

APPROXIMATIONS FOR DISTANCES SHORT OR LONG COMPARED WITH HEIGHT OF IONOSPHERE

The numerical results show that H_r varies as $1/r^3$ if $r \ll h$ and $1/r^2$ if $r \gg h$. The transition from spherical to cylindrical spreading

of the near field is to be expected; here we derive analytic expressions for that dependence.

As an example, we consider the case of a uniform earth of conductivity σ_1 and a perfectly conducting ionosphere. For that case, Eq. (A.14) becomes

$$H_r = -\frac{M}{2\pi}\cos\phi\int_0^\infty \frac{\gamma_1 e^{-\gamma_1 d}}{\lambda + \gamma_1 \tanh(\lambda h)}\left[J_0(\lambda r)\lambda - \frac{1}{r}J_1(\lambda r)\right]\lambda\, d\lambda \ . \quad (A.46)$$

This expression can be rewritten as

$$H_r = -\frac{M}{2\pi}\cos\phi\frac{d}{dr}I(r) \ , \quad (A.47)$$

where

$$I(r) = \frac{1}{r^2}\int_0^\infty \frac{\gamma_1' e^{-\gamma_1' d/r}}{t + \gamma_1' \tanh\left(\frac{th}{r}\right)} J_1(t)t\, dt \quad (A.48)$$

and

$$(\gamma_1')^2 = t^2 + k^2 r^2 \ .$$

Short-Range Approximation

If $r << h$ and $r << \delta_1$, where δ is the skin depth, we can write

$$\tanh\left(\frac{th}{r}\right) \approx 1 \quad (A.49)$$

and

$$\gamma_1' \approx t \ , \quad (A.50)$$

which simplifies Eq. (A.48) to

$$I(r) \approx \frac{1}{2r^2} \int_0^\infty e^{-td/r} J_1(t) t \, dt \, , \qquad r << h, \delta_1 \, . \tag{A.51}$$

The integral in Eq. (A.51) is a standard form [Gradshteyn and Ryzhik, 1980], yielding simply

$$I \approx \frac{r}{2R^3} \, , \tag{A.52}$$

where $R^2 = r^2 + d^2$. In all practical cases, $r >> d$, so Eq. (A.47) becomes

$$H_r \approx \frac{M}{2\pi r^3} \cos \phi \, , \qquad r << h, \delta_1 \, , \tag{A.53}$$

which is the well-known form for an HMD on a uniform half space [Kraichman, 1970].

Equation (A.53) is valid for ranges shorter than both the height of the ionosphere and the skin depth in the earth. It is most useful when the skin depth is comparable to or greater than the height of the ionosphere. Another simple expression applies when the skin depth is small and $\delta_1 << r << h$. Then we write

$$\tanh\left(\frac{th}{r}\right) \approx 1 \tag{A.54}$$

and

$$\gamma_1' \approx k_i \, , \tag{A.55}$$

which yield

$$I(r) \approx \frac{1}{r^2} \int_0^\infty e^{-td/r} J_1(t) t \, dt \tag{A.56}$$

and

$$H_r \approx \frac{M}{\pi r^3} \cos \phi \ , \qquad \delta_1 << r << h \ . \tag{A.57}$$

Equation (A.57) is a well-known expression for the field of an HMD on a highly conducting half space. Note that both Eqs. (A.53) and (A.57) predict an inverse-cube dependence on distance if the range is less than the effective height of the ionosphere.

Long-Range Approximation

If $r >> h$, we can write

$$\tanh\left(\frac{th}{r}\right) \approx \frac{th}{r} \tag{A.58}$$

and

$$(\gamma_1')^2 \approx \gamma_g^2 r^2 \approx -\frac{2ir^2}{\delta_1^2} \ , \tag{A.59}$$

which allow Eq. (A.48) to be rewritten as

$$I \approx \frac{1}{r} \frac{\gamma_g}{1 + \gamma_g h} \int_0^\infty J_1(t)\, dt = \frac{1}{r} \frac{\gamma_g}{1 + \gamma_g h} \ , \qquad r >> h \ , \tag{A.60}$$

where we have used $\gamma_g d << 1$. Insertion of Eq. (A.60) into Eq. (A.47) gives the following approximation for the magnetic field:

$$H_r \approx \frac{M \cos \phi}{2\pi r^2} \left(\frac{\sqrt{-2i}}{\delta_1 + \sqrt{-2i}\, h} \right), \qquad r >> h \ , \tag{A.61}$$

which, for a highly conducting earth, becomes

$$H_r \approx \frac{M \cos \phi}{2\pi h r^2} \ , \qquad r >> h >> \delta_1 \ . \tag{A.62}$$

These equations show that the field has an inverse-square dependence on range for distances greater than the height of the ionosphere.

Equations (A.57) and (A.62) can be combined to obtain the following heuristic form, which works well at nearly all ranges for a highly conducting earth:

$$H_r \approx \frac{M \cos \phi}{2\pi r^2} \left(\frac{r + 2h}{rh} \right) , \qquad \delta_1 << r, h . \tag{A.63}$$

NUMERICAL INTEGRATION OF SOMMERFELD INTEGRALS

Equations (A.14) through (A.19) contain the Sommerfeld integrals

$$S(\rho) = \int_0^\infty F(\lambda) J_m(\lambda\rho) \, e^{-g(\lambda)} \, d\lambda , \tag{A.64}$$

which normally converge very slowly. When the pathlength exceeds an attenuation length, the usual procedure is to evaluate the integrals in terms of residues, which give the familiar waveguide modes [Wait, 1970]. However, ULF wavelengths are so great that asymptotic waveguide theory is inapplicable, so we must proceed numerically.

Bubenik [1977] outlines a numerical method to integrate Sommerfeld integrals that is based on a nonlinear transformation of the sequence

$$S_n = \int_0^{z_n} F(\lambda) J_m(\lambda\rho) \, e^{-g(\lambda)} \, d\lambda , \qquad n = 1, 2, \ldots , \tag{A.65}$$

where z_n is the *nth* zero of J_m. That transformation, discussed by Shanks [1955], can be quickly computed using a method due to Wynn [1956]. We have developed and applied a code that uses the Shanks-Wynn algorithm to determine S while keeping the sequence $S_1, \ldots, S_n$ as short as possible.

REFERENCES

Bannister, P. R., *Scientific and Engineering Studies: Quasi-static Electromagnetic Fields,* Naval Underwater Systems Center, New London, Connecticut, 1980.

Bostick, F. X., C. S. Cox, and E. C. Field, "Land-to-Seafloor Electromagnetic Transmissions in the 0.1 to 15 Hz Band," *Radio Sci.*, Vol. 13, July-August 1978, pp. 701-708.

Bostick, F. X., H. W. Smith, and J. E. Boehl, *Magnetotelluric and DC Dipole-Dipole Resistivity Measurements in the Northern Olympic Peninsula,* University of Texas at Austin, Electrical Geophysical Laboratory, May 1977.

Bubenik, D. M., "A Practical Method for the Numerical Evaluation of Sommerfeld Integrals," *IEEE Trans. Antennas Propag.*, Vol. AP-25, No. 6, November 1977, pp. 904-906.

Fraser-Smith, A. C., and D. M. Bubenik, *Compendium of the ULF/ELF Electromagnetic Fields Generated above a Sea of Finite Depth by Submerged Harmonic Dipoles,* Stanford Electronics Laboratories, Technical Report E715-1 (SEL 79-025), January 1980.

Gradshteyn, I. S., and I. M. Ryzhik, *Table of Integrals, Series, and Products,* trans. by Scripta Technica, Inc., Alan Jeffrey (ed.), Academic Press, New York, 1980.

Greifinger, C., and P. Greifinger, "Theory of Hydromagnetic Propagation in the Ionospheric Waveguide," *J. Geophys Res.*, Vol. 73, No. 23, December 1968, pp. 7473-7490.

-----, *Feasibility of ULF Communication via Earth-Ionospheric Waveguide,* R & D Associates, Marina del Rey, California, RDA-TR-4600-005, July 1974.

Kraichman, M. B., *Handbook of Electromagnetic Propagation in Conducting Media,* U.S. Naval Ordnance Laboratory, Silver Spring, Maryland (USGPO, Washington, D.C.), 1970.

Shanks, D., "Non-Linear Transformations of Divergent and Slowly Convergent Sequences," *J. Math. Phys.*, Vol. 34, 1955, pp. 1-42.

Sommerfeld, A., *Partial Differential Equations in Physics,* Academic Press, New York, 1949, p. 335.

Wait, J. R., *Electromagnetic Waves in Stratified Media,* Pergamon Press, New York, 1970, p. 608.

Wynn, P., "On a Device for Computing the e_m (S_n) Transformation," *Math. Tables Other Aids Comp.*, Vol. 10, 1956, pp. 91-96.